ISSN 1674-1056
http://cpb.iphy.ac.cn
http://iopscience.iop.org/cpb
中国物理 B
Chinese Physics
中国物理 Chinese Physics B

Structural, mechanical and electronic properties of 25 kinds of *III-V* binary monolayers:A computational investigation with first-principle calculation

Xue-Fei Liu(刘雪飞), Zi-Jiang Luo(罗子江), Xun Zhou(周勋), Jie-Min Wei(魏节敏), Yi Wang(王一), Xiang Guo(郭祥), Bing Lv(吕兵), Zhao Ding(丁召)

Citation: Chin. Phys. B . 2019, 28(8): 086105. **doi:** 10.1088/1674-1056/28/8/086105
Journal homepage: http://cpb.iphy.ac.cn; http://iopscience.iop.org/cpb

What follows is a list of articles you may be interested in

Structural and electrical properties of Ga-Te systems under high pressure

Youchun Wang(王友春), Fubo Tian(田夫波), Da Li(李达), Defang Duan(段德芳), Hui Xie(谢慧), Bingbing Liu(刘冰冰), Qiang Zhou(周强), Tian Cui(崔田)

Chin. Phys. B . 2019, 28(5): 056104. **doi:** 10.1088/1674-1056/28/5/056104

Bandgap engineering to tune the optical properties of $Be_xMg_{1-x}X$ (X=S, Se, Te) alloys

B Sabir, N A Noor, M Rashid, Fasih Ud Din, Shahid M Ramay, Asif Mahmood

Chin. Phys. B . 2018, 27(1): 016101. **doi:** 10.1088/1674-1056/27/1/016101

Density functional study on the pressure profile of the inhomogeneous fluid mixture

Yanshuang Kang(康艳霜), Yanmei Kang(康艳梅), Zongli Sun(孙宗利), Yushan Li(李玉山), Shanshan Tan(檀姗姗)

Chin. Phys. B . 2017, 26(8): 086101. **doi:** 10.1088/1674-1056/26/8/086101

High-pressure structure and elastic properties of tantalum single crystal: First principles investigation

Jian-Bing Gu(顾建兵), Chen-Ju Wang(王臣菊), Wang-Xi Zhang(张旺玺), Bin Sun(孙斌), Guo-Qun Liu(刘国群), Dan-Dan Liu(刘丹丹), Xiang-Dong Yang(杨向东)

Chin. Phys. B . 2016, 25(12): 126103. **doi:** 10.1088/1674-1056/25/12/126103

Theoretical calculations of structural, electronic, and elastic properties of $CdSe_{1-x}Te_x$: A first principles study

M Shakil, Muhammad Zafar, Shabbir Ahmed, Muhammad Raza-ur-rehman Hashmi, M A Choudhary, T Iqbal

Chin. Phys. B . 2016, 25(7): 076104. **doi:** 10.1088/1674-1056/25/7/076104

Structural, mechanical, and electronic properties of 25 kinds of *III–V* binary monolayers: A computational study with first-principles calculation*

Xue-Fei Liu(刘雪飞)[1,2,3], Zi-Jiang Luo(罗子江)[1,2,4], Xun Zhou(周勋)[3], Jie-Min Wei(魏节敏)[1,2,5], Yi Wang(王一)[1,2], Xiang Guo(郭祥)[1,2], Bing Lv(吕兵)[3], and Zhao Ding(丁召)[1,2,†]

[1] *College of Big Data and Information Engineering, Guizhou University, Key Laboratory of Micro-Nano-Electronics of Guizhou Province, Guiyang* 550025, *China*

[2] *Semiconductor Power Device Reliability Engineering Center of Ministry of Education, Guiyang* 550025, *China*

[3] *College of Physics and Electronic Science, Guizhou Normal University, Guiyang* 550025, *China*

[4] *College of Information, Guizhou Finance and Economics University, Guiyang* 550025, *China*

[5] *Guizhou Institute of Technology, Guiyang* 550002, *China*

(Received 10 April 2019; revised manuscript received 20 May 2019; published online 9 July 2019)

Using first-principle calculations, we investigate the mechanical, structural, and electronic properties and formation energy of 25 kinds of *III–V* binary monolayers in detail. A relative radius of the binary compound according to the atomic number in the periodic table is defined, and based on the definition, the 25 kinds of *III–V* binary compounds are exactly located at a symmetric position in a symmetric matrix. The mechanical properties and band gaps are found to be very dependent on relative radius, while the effective mass of holes and electrons are found to be less dependent. A linear function between Young's modulus and formation energy is fitted with a linear relation in this paper. The change regularity of physical properties of B–*V* (*V* = P, As, Sb, Bi) and *III*–N (*III* = Al, Ga, In, Tl) are found to be very different from those of other *III–V* binary compounds.

Keywords: density functional theory, *III–V* binary, monolayers, band structure, mechanical properties

PACS: 61.72.uj, 73.20.At, 73.61.Ey, 73.90.+f **DOI:** 10.1088/1674-1056/28/8/086105

1. Introduction

At present, *III–V* compound semiconductors provide the material basis for a number of well-established commercial technologies, and have applications in electronic and optoelectronic devices,[1] especially in lasers,[2] light-emitting diodes (LEDs),[3] solar cells,[4] and photodetectors.[5] During the past decades, most research has been done with *III–V* material systems. Kim *et al.* have studied the elastic constants and related properties of tetrahedrally bonded BN, AlN, GaN and InN systematically, and they obtained some important conclusions about the four binary alloys.[6] In 1999, Kern *et al.* obtained the phase diagram of boron nitride via ab initio calculation.[7]The band parameters for 13 kinds of *III–V* semiconductor alloys have been calculated in Ref. [1] with the $K\cdot$P method. However, all of the studies were mainly engaged in the bulk phase of *III–V* materials.[8] In 2004, Novoselov *et al.* produced graphene by mechanical exfoliation of graphite and proved many excellent properties existing in this strict two-dimensional (2D) monolayer material.[9] From then on, more and more research has been focused on the free-standing 2D material systems, both theoretically and experimentally.[10–14] In 2D *III–V* material systems, BN[14,15] and phosphorene[16–18] are the most intensively studied ones; GaN, AlN, GaAs, GaSb, and GaP are also studied by researchers,[19–21], who have proven that the physical properties of *III–V* alloys would be very different from those of bulk ones. Based on density functional theory (DFT), many aspects have been studied for 2D *III–V* materials, such as the effects of the strain and external electric field on the electronic properties,[20] intrinsic defect formation energy in BN bilayer and monolayer,[22] the tuning of the band gap of $In_xGa_{1-x}N$ by changing the number of layers,[23] the mechanical anisotropy and lattice defects of borophene,[24] and the structural and electronic properties of B_2N_3.[25] These studies, which mainly focus on some important physical properties of one or several kinds of *III–V* 2D materials in the case of some external factors, are introduced. To the best of our knowledge, few publications are found to compare and study the regularity of certain properties systematically under the conditions with or without stress for all 25 kinds of *III–V* 2D binary alloys *AB* (*A* = boron, aluminum, gallium, indium, thallium, and *B* = nitrogen, phosphorus, arsenic, Sb (antimony), bismuth). We speculate that by comparing these 25 kinds of 2D materials together, some important regularities behind the physical properties could be found more clearly and intuitively, significant for finding some new 2D materials used in various fields, as well as guiding the experimenters in choosing the combinations of two or more elements which would prepare better

*Project supported by the National Natural Science Foundation of China (Grant Nos. 61564002 and 11664005), the Guizhou Normal University Innovation and Entrepreneurship Education Research Center Foundation (Grant No. 0418010), and the Joint Foundation of Guizhou Normal University (Grant No. 7341).

†Corresponding author. E-mail: zding@gzu.edu.cn

© 2019 Chinese Physical Society and IOP Publishing Ltd

material. Motivated by this, we calculate all *III–V* 2D materials by first-principles method. The remainder of this paper is organized as follows, methodology and computational details are described in Section 2. In Section 3 the calculations of band structures, effective mass of electrons and holes at band edges and elastic properties are presented. Finally, some conclusions are briefly summarized in Section 4.

2. Computational details

All of calculations in this paper were performed using the Vienna *Ab initio* Simulation Package (VASP).[26,27] The interaction between electrons and ions was described by the projector augmented wave (PAW) method[28] and the exchange and correlation were treated with generalized gradient approximation (GGA) at the Perdew–Burke–Ernzerhof (PBE) level.[29] By a cutoff energy convergence test from 300 eV to 450 eV for all binary *III–V* compounds with an energy and force convergence 10^{-5} eV/atom and 0.02 eV/Å respectively, we adopted 450 eV for ENCUT during all calculations, which yielded a total energy convergence better than 0.001 eV/atom. The Brillouin zone was sampled by a Γ-centered Monkhorst–Pack $23 \times 23 \times 1$ k-mess based on a convergence test.[30] In order to eliminate the mirror interactions induced by periodic boundary, a 15-Å vacuum layer in the c direction was constructed. All slabs were obtained by cleaving a (111) surface from a bulk structure and translated to a primitive cell with a monolayer; afterwards the lattice constants were fitted by equation of state (EOS) with the Birch–Murnaghan 3rd-order method.[31] The GGA-PBE level exchange–correction usually underestimate the band gap of the calculated materials system, which will lead to worse results if one wishes to analyze the optical properties or defect formation energy for a given material.[32,33] Therefore, a hybrid density functional proposed by Heyd, Scuseria, and Ernzerhof (HSE) would be a better choice.[34] However, we still used a standard GGA-PBE level to carry out most of our calculations except for the band structures without strain for the reasons that this paper aims to investigate some variation trends of all *III–V* binary material systems under certain conditions, which means that qualitative analyses are enough. Additionally, on the other hand, a hybrid method is too expensive for us to calculate 25 kinds of *III–V* binary alloys under different strains in different directions. Additionally, standard DFT or hybrid DFT both failed to describe the weakly bound systems such as layered 2D materials where van der Waals (vdW) interactions are a dominant part in the cohesive energy,[24] in which case, a semi-empirical correction scheme (DFT-D2/D3) proposed by Grimme can be used to treat the weak interactions.[35] In this paper, we mainly investigate the electronic and mechanical properties, bonds and effective mass at band edge based on standard DFT methods.

3. Results and discussion

3.1. Structural properties

In order to clearly describe the structures used in this paper, a 4×4 AlBi supercell is used as a template structure and illustrated in Fig. 1. We note that all other 24 kinds of binary alloys have a similar structure as shown in Fig. 1 and for all calculations the primitive cell is used.

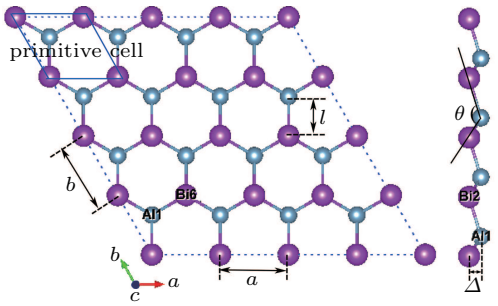


Fig. 1. Top (left) and side (right) view of template structure (AlBi) used in this paper, with lattice constant denoting as a and b ($a = b$), and l, Δ, and θ representing bond length, buckling constant, and bond angle respectively.

The calculated lattice constant (a), bond length (l), buckling constant (Δ), bond angle (θ), formation energy (E_f), band gap (E_g), effective mass of electrons (m_e^*/m_0^*) , effective mass of holes (m_h^*/m_0^*) and the band gap types (D/ID), where D and ID represent the direct and indirect energy band gap respectively, are listed in Table 1 and divided into five groups according to the V atoms. One can find that for *III–V* binary compounds (*III* = B, Al, Ga, In, Tl, *V* = N, P, As, Sb, Bi), both the lattice constant and bond length increase unsurprisingly with the radius of atom increasing, and the lattice parameters of GaN, GaP, GaAs, and GaSb are consistent with those in Refs. [20] and [36] with a small error of less than 1%, and the lattice constant of bulk h-BN in Ref. [37] from first principles method is 2.494 Å, which is underestimated only by 0.7% compared with our results. According to our calculations, of 25 kinds of binary *III–V* compounds, 7 kinds of binary compounds have a planar structure similar to graphene. *i.e.*, BN, AlN, GaN, InN, BP, BAs, and BSb are optimized into a planar monolayer structure, and the results are in compliance with those in Ref. [38]; in addition, TlN and AlP are very inclined to forming flat structures with a bond angle 119.921° and 119.407° respectively. It can be concluded that the smaller the lattice constant, the easier the planar structure to be formed. To be more precise, the lattice constant and bond length of a planar monolayer must be smaller than 3.74 Å and 2.16 Å for an *III–V* binary respectively. We note that all *X*N (*X* = B, Al, Ga, In, Tl) and B*Y* (*Y* = N, P, As, Sb, except for Bi) 2D compounds tend to be planarized due to the lattice constants and bond lengths are smaller than 3.74 Å and 2.16 Å respectively. Conversely, there are 16 kinds of *III–V* compounds with a buckling structure due to a larger dimension and the buckling constant (Δ) that represents the degree of buckling. Also, we calculate the formation energy for all binary compounds from the following formula:

$$E_f^{III-V} = E_{tot}^{III-V} - E_{tot}^{III} - E_{tot}^{V}, \quad (1)$$

where $E_{\rm f}^{III-V}$, $E_{\rm tot}^{III-V}$, $E_{\rm tot}^{III}$, and $E_{\rm tot}^{V}$ are the formation energy, energy of monolayer *III*–*V* binary, *III* atom energy, and *V* atom energy respectively, the formation energy of GaN, GaP, GaAs, and GaSb are −8.122, −5.201, −4.391, and −3.870 eV,[20] respectively and are very close to our results in Table 1. Obviously, the formation energy in the same group (*i.e.*, a given *V* atom) and different groups (*i.e.* a given *III* atom) both increase with the increase of radii of *V* and *III* atoms. As a more negative formation energy means a more favored stable structure, a conclusion can be drawn that a smaller atom is beneficial to not only the formation of a planar structure, but also to a layered 2D structure, which is consistent with the results of mechanical properties as shown in the next section. As analyzed above, that the *III*–Ns and B–*V*s (except for BBi) are favored in energy to form a planar monolayer can be explained by the fact that they have a smaller formation energy.

Table 1. Values of optimized lattice constant (a), bond length (l), buckling constant (Δ), bond angle (θ), formation energy ($E_{\rm f}$), band gap ($E_{\rm g}$), effective mass of electrons ($m_{\rm e}^*/m_0^*$), effective mass of holes ($m_{\rm h}^*/m_0^*$), and band gap types (D/ID), with D and ID representing direct and indirect energy band gap respectively.

Monolayer	a/Å	l/Å	Δ/Å	$\theta/(^\circ)$	$E_{\rm f}$/eV	$E_{\rm g}$/eV		$m_{\rm e}^*/m_0^*$		$m_{\rm h}^*/m_0^*$		Band type (D/ID)
						HSE06	PBE					
BN	2.514	1.451	0.001	120.000	–13.338	5.67	4.65	$K\to M$	1.084	$K\to M$	–0.520	D
								$K\to\Gamma\to\Gamma$	0.799	$K\to\Gamma$	–0.667	
AlN	3.127	1.805	0.001	119.999	–10.168	4.04	2.91	$\Gamma\to K$	0.494	$K\to M$	–1.487	ID
								$\Gamma\to M$	0.494	$K\to\Gamma$	–1.213	
GaN	3.210	1.853	0.000	120.000	–7.594	3.43	2.16	$\Gamma\to K$	0.233	$K\to M$	–1.846	ID
								$\Gamma\to M$	0.153	$K\to\Gamma$	–1.439	
InN	3.586	2.071	0.001	120.000	–6.052	1.61	0.56	$\Gamma\to K$	0.079	$\Gamma\to K$	–1.471	D
								$\Gamma\to M$	0.079	$\Gamma\to M$	–1.485	
TlN	3.730	2.155	0.061	119.921	–4.402	0.14	0.00	$\Gamma\to K$	0.139	$\Gamma\to K$	–0.724	D
								$\Gamma\to M$	0.129	$\Gamma\to M$	–0.531	
BP	3.200	1.847	0.005	119.999	–9.096	1.36	0.89	$K\to M$	0.225	$K\to M$	–0.203	D
								$K\to\Gamma$	0.192	$K\to\Gamma$	–0.174	
AlP	3.933	2.277	0.176	119.407	–6.726	3.21	2.37	$M\to\Gamma$	0.477	$K\to M$	–0.914	ID
								$M\to K$	0.190	$K\to\Gamma$	–0.763	
GaP	3.897	2.282	0.382	117.255	–5.540	2.61	1.64	$\Gamma\to K$	0.098	$K\to M$	–0.706	ID
								$\Gamma\to M$	0.129	$K\to\Gamma$	–0.614	
InP	4.221	2.489	0.506	115.974	–4.934	1.90	1.08	$\Gamma\to K$	0.090	$K\to M$	–0.832	ID
								$\Gamma\to M$	0.090	$K\to\Gamma$	–0.737	
TlP	4.316	2.561	0.592	114.820	–3.970	0.80	0.22	$\Gamma\to K$	0.036	$\Gamma\to K$	–0.610	D
								$\Gamma\to M$	0.037	$\Gamma\to M$	–0.592	
BAs	3.391	1.958	0.012	119.995	–7.716	1.20	0.75	$K\to M$	0.188	$K\to M$	–0.180	D
								$K\to\Gamma$	0.162	$K\to\Gamma$	–0.157	
AlAs	4.056	2.388	0.459	116.263	–5.910	2.52	1.73	$\Gamma\to K$	0.137	$K\to M$	–0.749	ID
								$\Gamma\to M$	0.137	$K\to\Gamma$	–0.643	
GaAs	4.053	2.410	0.578	114.446	–4.920	1.85	1.05	$\Gamma\to K$	0.068	$K\to M$	–0.632	ID
								$\Gamma\to M$	0.068	$K\to\Gamma$	–0.546	
InAs	4.363	2.603	0.655	113.891	–4.496	1.44	0.77	$\Gamma\to K$	0.063	$\Gamma\to K$	–0.636	D
								$\Gamma\to M$	0.063	$\Gamma\to M$	–0.644	
TlAs	4.480	2.678	0.694	113.525	–3.719	0.46	0.00	$\Gamma\to K$	0.709	$\Gamma\to K$	–0.590	D
								$\Gamma\to M$	0.711	$\Gamma\to M$	–0.572	
BSb	3.738	2.158	0.033	119.977	–6.525	0.62	0.32	$K\to M$	0.115	$K\to M$	–0.112	D
								$K\to\Gamma$	0.107	$K\to\Gamma$	–0.106	
AlSb	4.401	2.616	0.623	114.517	–5.026	1.97	1.24	$\Gamma\to K$	0.095	$K\to M$	–0.611	ID
								$\Gamma\to M$	0.096	$K\to\Gamma$	–0.520	
GaSb	4.380	2.626	0.710	112.973	–4.314	1.51	0.84	$\Gamma\to K$	0.053	$K\to M$	–0.508	ID
								$\Gamma\to M$	0.053	$K\to\Gamma$	–0.438	
InSb	4.678	2.805	0.759	112.967	–4.027	1.32	0.67	$\Gamma\to K$	0.054	$K\to M$	–0.623	ID
								$\Gamma\to M$	0.053	$K\to\Gamma$	–0.540	
TlSb	4.790	2.874	0.782	112.881	–3.429	0.63	0.00	$\Gamma\to K$	0.543	$\Gamma\to K$	–0.511	D
								$\Gamma\to M$	0.548	$\Gamma\to M$	–0.517	
BBi	3.877	2.289	0.480	115.718	–5.617	0.86	0.50	$K\to M$	0.187	$K\to M$	–0.176	D
								$K\to\Gamma$	0.162	$K\to\Gamma$	–0.156	
AlBi	4.513	2.717	0.771	112.282	–4.563	1.38	0.79	$\Gamma\to K$	0.055	$\Gamma\to K$	–0.592	D
								$\Gamma\to M$	0.055	$\Gamma\to M$	–0.590	
GaBi	4.521	2.727	0.821	111.939	–4.027	0.50	0.00	$\Gamma\to K$	0.037	$\Gamma\to K$	–0.517	D
								$\Gamma\to M$	0.037	$\Gamma\to M$	–0.518	
InBi	4.809	2.906	0.859	111.651	–3.786	0.65	0.17	$\Gamma\to K$	0.033	$\Gamma\to K$	–0.557	D
								$\Gamma\to M$	0.036	$\Gamma\to M$	–0.556	
TlBi	4.928	2.970	0.852	112.114	–3.314	–0.02	0.00	$\Gamma\to K$	0.05	$\Gamma\to K$	–0.549	D (metal)
								$\Gamma\to M$	0.05	$\Gamma\to M$	–0.541	

3.2. Mechanical properties

We calculate the mechanical parameters such as stiffness constants C_{ij} (GPa·nm·N/m), $i, j = 126$ Young's modulus Y_k $(\mathrm{GPa}\cdot\mathrm{nm}, \mathrm{N/m})$ $k = x, y$, shear modulus S (GPa, nm, N/m), and Poisson's ratio of all 25 kinds of *III–V* binary 2D monolayers. For a 2D structure, the relation between stress and strain can be derived based on Hooke's law under in-plane stress conditions as follows:[24]

$$\begin{bmatrix} \sigma_{xx} \\ \sigma_{yy} \\ \sigma_{xy} \end{bmatrix} = \begin{bmatrix} C_{11} & C_{12} & 0 \\ C_{12} & C_{22} & 0 \\ 0 & 0 & C_{66} \end{bmatrix} \begin{bmatrix} \varepsilon_{xx} \\ \varepsilon_{yy} \\ 2\varepsilon_{xy} \end{bmatrix}. \tag{2}$$

Here, C_{ij} is the second partial derivative of strain energy E_s with respect to strain ε, corresponding to the component of the elastic modulus tensor, and can be written as

$$C_{ij} = \left(\frac{1}{\mathrm{S}_0}\right)\left(\frac{\partial^2 E_\mathrm{s}}{\partial\varepsilon_i \partial\varepsilon_j}\right). \tag{3}$$

S_0 is the equilibrium area of the crystal. In a general way used in ab-initio calculations for a 2D material, E_s is determined by formula (4) using the standard Voigt notation,[39]

$$E_S = \frac{1}{2}C_{11}\varepsilon_{xx}^2 + \frac{1}{2}C_{22}\varepsilon_{yy}^2 + C_{12}\varepsilon_{xx}\varepsilon_{yy} + 2C_{66}\varepsilon_{xy}^2. \tag{4}$$

In the calculations, we define the strain $\varepsilon = (b - b_0)/bb$ and b_0 as the lattice constant with and without strain, respectively. For the uniaxial and equi-biaxial strain, we apply a finite scaling to the $\boldsymbol{x}(\boldsymbol{y})$ and $(\boldsymbol{x}, \boldsymbol{y})$ direction, where $\boldsymbol{x}$ is chosen to be along lattice $\boldsymbol{a}$ vector (zigzag) and $\boldsymbol{y}$ (armchair) to be perpendicular to $\boldsymbol{x}$. The most favorable structure in energy is set to be the strain-free structure and the strain range along the corresponding direction changes from -2.5% to 2.5% in steps of 0.5%. The shear strain is also considered in this paper, which means that we will do the calculations 44 times for each binary monolayer in order to obtain the elastic constants by fitting the data of elastic strain energy $E_\mathrm{s}(\varepsilon)$ as a function of strain ε using a quadratic polynomial. After that, the Young's modulus Y and Poisson's ratio υ can be derived as[40]

$$Y_x = \frac{C_{11}C_{22} - C_{12}C_{21}}{C_{22}}, \quad Y_y = \frac{C_{11}C_{22} - C_{12}C_{21}}{C_{11}}, \tag{5}$$

$$\upsilon_x = \frac{C_{21}}{C_{22}}, \quad \upsilon_y = \frac{C_{12}}{C_{11}}. \tag{6}$$

Noting that the shear modulus (S) of a 2D crystal can be obtained directly based on C_{66} ($S = C_{66}$), by using a post-processing VASPKIT code,[33] the stiffness constants, Young's modulus, shear modulus and Poisson's ratio are obtained as listed in Table 2.

Table 2. Calculated elastic stiffness constants C_{ij} (GPa, nm, N/m), $i, j = 126$, Young's modulus Y_k (GPa·nm, N/m), $k = xy$, shear modulus S (GPa, nm, N/m), and Poisson's ratio ν_k, $k = x, y$.

Monolayer	Stiffness tensor/(N/m)				Young's modulus/(N/m)		Shear modulus/(N/m)	Poisson's ratio	
	C_{11}	C_{22}	C_{12}	C_{66}	Y_x	Y_y	S	ν_x	ν_y
BN	290.666, 293.1[42]	290.085	65.277, 63.76[42]	112.873	275.977, 279.2[42]	275.425	112.873	0.225, 0.21[38]	0.225
AlN	143.792	142.948	66.227	39.176	113.109	112.446	39.176	0.463, 0.46[38]	0.461
GaN	133.201, 110[38]	132.277	59.335	37.871	106.586	105.846	37.871	0.449	0.445
InN	92.875	93.687	54.113	20.648	61.619	62.158	20.648	0.578, 0.59[38]	0.583
TlN	61.986	61.857	85.102	9.645	-55.095	-54.98	9.645	1.376	1.373
BP	150.788	151.17	41.777	54.491	139.243	139.596	54.491	0.276, 0.28[38]	0.277
AlP	71.423	71.261	22.325	19.846	64.429	64.283	19.846	0.313	0.313
GaP	64.38	64.822	19.75	21.397	58.363	58.763	21.397	0.305	0.307
InP	46.792	46.459	17.867	14.254	39.92	39.637	14.254	0.385	0.382
TlP	36.816	37.083	29.372	10.679	13.553	13.651	10.679	0.792	0.798
BAs	126.279	126.115	35.591	45.589	116.235	116.084	45.589	0.282, 0.29[38]	0.282
AlAs	53.004	53.006	18.124	17.186	46.807	46.809	17.186	0.342	0.342
GaAs	48.981, 48[38]	48.871	16.009	16.473	43.737	43.638	16.473	0.328	0.327
InAs	36.969, 33[38]	36.751	14.171	11.122	31.505	31.319	11.122	0.386	0.383
TlAs	26.16	26.022	15.22	6.571	17.258	17.167	6.571	0.585	0.582
BSb	94.084	94.823	31.101	32.942	83.883	84.542	32.942	0.328, 0.34[38]	0.331
AlSb	37.249, 35[38]	37.176	11.844	11.98	33.475	33.41	11.98	0.319	0.318
GaSb	32.529	32.986	12.821	11.329	27.546	27.933	11.329	0.389	0.394
InSb	28.184	28.68	9.306	8.421	25.164	25.608	8.421	0.324	0.33
TlSb	21.472	20.627	39	5.182	-52.265	-50.207	5.182	1.891	1.816
BBi	66.924	66.724	19.788	23.584	61.055	60.873	23.584	0.297	0.296
AlBi	31.055	31.266	11.563	9.819	26.779	26.961	9.819	0.37	0.372
GaBi	20.898	20.971	20.781	6.096	0.305	0.306	6.096	0.991	0.994
InBi	24.808	24.421	10.21	6.747	20.539	20.219	6.747	0.418	0.412
TlBi	17.241	17.077	12.489	3.524	8.108	8.031	3.524	0.731	0.724

For simplicity, we choose five kinds of binary monolayers as representatives, and the curves of strain-energy versus strain are presented in Fig. 2, *i.e.*, BN, AlP, GaAs, InSb, TlBi are intentionally chosen to include all elements in *III–V* column, and the ε_{xx}, ε_{yy}, $\varepsilon_x = \varepsilon_y$, and ε_{xy} are the uniaxial strain in the x direction, the uniaxial strain in the y direction, the equi-biaxial strain, and the shear strain respectively. It can be seen from Fig. 2 that the strain energy values of all binary compounds are almost symmetrical for compression (-2.5% to 0) and tension (0 to 2.5%) for all types of strain except that for AlP, and the non-symmetrical results of strain energy are found in GaBi, AlSb, and BP as well as among other 20 kinds of monolayers (not shown here). The results for BN in the same strain range are in accord with those of Ref. [41], where the total strain range is much larger than ours, and it shows that the symmetry is broken in a larger strain region. The results also show that all monolayer structures, except for InSb, under a small strain are isotropic due to the same strain energy response to the strain in the x direction and that in the y direction. The stiffness of C_{11}, C_{12}, and Young's modulus in Ref. [41] are, respectively, 293.1, 63.76, and 279.2 (N/m), which are much more consistent with our results listed in Table 2. The Poisson's ratio and stiffness of BN, BP, AlAs, *etc*. as listed in Table 2 are also in agreement with those of in Ref. [38], which means that our calculations are convincing and some regularity hence can be concluded by comparing all 25 kinds of binary compounds. Firstly, all mechanical constants except Poisson's ratio for all cases decrease with the increase of atom radius, *i.e.*, for a given group III element and changing of a group V element into a larger one or smaller one, the mechanical property is very sensitive to the dimension of lattice. Secondly, it is noteworthy that Young's modulus varies over a large range, *i.e.*, from a minimum value 0.306 N/m for GaBi to a maximum value 275.977 N/m for BN, which means that we can tune the mechanical property of 2D *III–V* binary materials very flexibly by combining different *III–V* elements into a binary compound or by dosing different elements into a binary compound to improve the elastic nature. For a mechanically stable 2D sheet, the Young's modulus and shear modulus must be larger than zero, *i.e.*, $C_{11}C_{22} - C_{12}^2 > 0$ and $C_{66} > 0$. Based on the simple criteria, TlSb and TlN with a Young's modulus of -55 N/m and -52 N/m respectively are the only two mechanically unstable binary compounds in *III–V*; at least they are less stable than other binary monolayer structures if the calculation error is taken into consideration. In order to investigate the qualitative relation between an atomic radius and the elastic constant, we assume the relative radius of B, Al, Ga, In, and Tl to be 5, 13, 31, 49, 81 and 7, 15, 33, 51, 83 for N, P, As, Sb, and Bi respectively. The reason for making the above assumption of relative radius for each element can be simply understood from the relative location in the periodic table. Based on the assumption, the radii of all binary compounds are summarized in Table 3.

Table 3. Assumed relative radius of each element and binary monolayer.

Binary	radius					
BN	12		N(7)	P15)	As(33)	Sb(51)	Bi(83)
AlN	20						
BP	20						
AlP	28						
GaN	38	B(5)	BN12	BP20	BAs38	BSb 56	BBi 8
BAs	38						
GaP	46						
AlAs	46						
InN	56	Al(13)	AlN20	AlP28	AlA 46	AlSb64	AlB 96
BSb	56						
InP	64						
GaAs	64						
AlSb	64						
InAs	82	Ga(31)	GaN 38	GaP 46	GaAs 64	GaSb 82	GaBi 114
GaSb	82						
TlN	88						
BBi	88						
TlP	96	In(49)	InN56	InP64	InAs82	InSb100	InBi132
AlBi	96						
InSb	100						
TlAs	114						
GaBi	114	Tl(81)	TlN88	TlP96	TlAs114	TlSb132	TlBi164
TlSb	132						
InBi	132						
TlBi	164						

It is interesting that the relative radii of 25 kinds of binary compounds form a perfect symmetric matrix, *e.g.*, AlN and BP, GaN, and BAs., which are symmetric about the main diagonal with a relative radius of 20 and 38, respectively.

The Poisson's ratio, shear modulus, and Young's modulus as a function of relative radius are illustrated in Fig. 3. Note that TlN and TlSb with a negative Young's modulus are excluded from the plot. As shown from Fig. 3, the shear modulus and Young's modulus have a total decreasing trend with the increase of the relative radius, whereas the Poisson's ratio is more complicated. However, it is interesting that all three mechanical constants will have a relatively big change at the boundary of different radius, *e.g.*, from 28 to 38, 38 to 46, 46 to 56, 56 to 64, 82 to 88, 88 to 96, 96 to 100, and 114 to 132, and each of the elastic natures of different binary compounds with the same radius almost keep a relatively stable value (*e.g.*, see the region denoted by blue rectangle). As seen from Fig. 3, BN has the largest shear and Young's modulus in all *III–V* binary monolayer compounds due to its smallest radius. From this point we can speculate that some structures formed by B, C, and N elements with a close relative radius will be beneficial to the improvement of the mechanical property, such as borophene grown successfully on Ag

(111) surface due to its extraordinary anisotropic mechanical properties.[24] The results[42] show that C_3 N monolayer can withstand up to strain level of 12% for zigzag and armchair uniaxial strain and 10% for *ab* biaxial strain. Li found that B_8 C_{12} is a new stable structure and is expected to be synthesized experimentally by using first-principles calculations.[43] Finally, it is worth noting that under a given relative radius, the binary compounds with a boron element show a slightly bigger shear and Young's modulus than those of other binary compounds with the same radius, *e.g.*, BP under radius = 20, BAs under radius = 38, BSb under radius = 56, and BBi under radius = 88, which validates the speculation above. Whether these binary compounds located in a symmetric region in Table 3 have any other similar properties is left for future study.

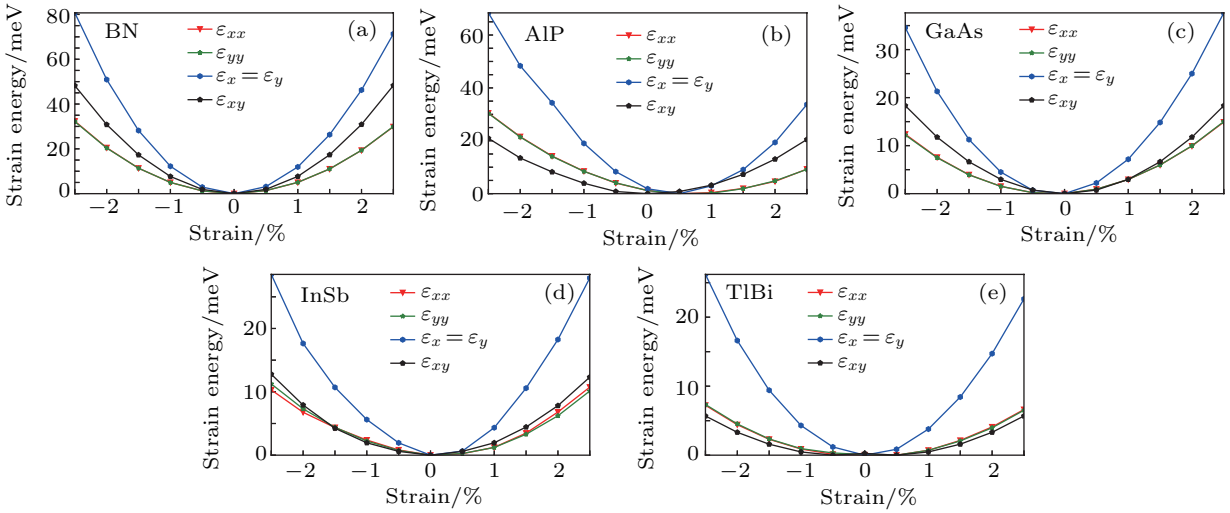


Fig. 2. Plots of ε_{xx} (uniaxial strain in *x* direction), ε_{yy} (uniaxial strain in *y* direction), $\varepsilon_x = \varepsilon_y$ (equi-biaxial strain), and ε_{yy} (shear strain) *versus* strain for (a) BN, (b) AlP, (c) GaAs, (d) InSb, and (e) TlBi, respectively.

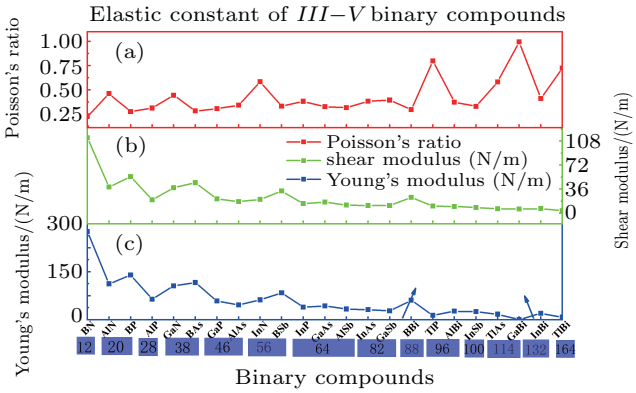


Fig. 3. Plots of (a) Poisson's ratio, (b) shear modulus, and (c) Young's modulus *versus* relative radius.

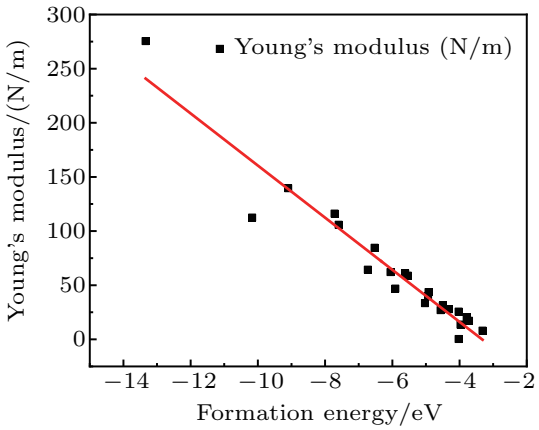


Fig. 4. Young's modulus as a function of formation energy.

By analyzing the results of formation energy and Young's modulus for all 25 kinds of binary compounds in *III–V*, we find an approximate linear relationship between the two physical quantities, and it is fitted to the following formula

$$Y = -24E - 80, \tag{7}$$

where Y and E are the Young's modulus and formation energy respectively. The Young's modulus as a function of formation energy is shown in Fig. 4.

3.3. Electrical properties

After analyzing the mechanical properties of those 25 kinds of *III–V* binary monolayer compounds, we start to investigate the electronic properties. We calculate the band structures, density of states, and band edge carrier effective mass for all *III–V* binary monolayer compounds respectively under uniaxial, equi-biaxial strained, and free-strained conditions at the PBE level. Since the band gaps of semiconductors are often underestimated by the standard density functional theory (DFT), the band structures of 25 kinds of binary compounds without strain are calculated by using the Heyd–Scuseria–Ernzerhof (HSE06) hybrid functional[34,44–47] for more rigorous scrutiny, during all calculations the screening parameter and the Hartree–Fock (HF) mixing parameter are chosen to be $\mu = 0.2$ Å^{-1} and $\alpha = 25\%$ respectively. The band gaps calculated with the PBE and HSE06 levels, effective

mass of the electron at the conduction band minimum (CBM) and the hole at the valence band maximum (VBM) are listed in Table 1, and the band gap types listed in Table 1 are denoted as D for a direct gap and ID for an indirect one, respectively. We note that the effective mass of carrier is calculated using PBE only by trading off the calculation time. More importantly, the shape of the band structure from PBE always changes a little compared with that of HSE06, and the effective mass is mainly determined by the shape of the band structure rather than the band gap by using a parabola fitting method.[23] As seen from Table 1, the band gap values of GaN, GaP, GaAs, and GaSb with PBE are 2.16, 1.64, 1.05, and 0.84 eV respectively, which are in agreement with those in Ref. [20], where the corresponding band gap values are 1.85, 1.56, 1.31, and 0.79 eV respectively. The underestimated band gaps are improved by the HSE06 method as shown in Table 1. The band gap of GaN calculated by HSE06 is 3.43 eV, which is very close to the experimental value 3.50 eV, and the experimental values of effective mass of the electron and hole are 0.18 and $1.64m_0$, which are also in agreement with the average values of our results.[23] However, the band gap of InN of a monolayer is 1.61 eV (HSE06) and is much larger than the experimental value (0.70 eV) in a bulk InN material. Our results for band gap values for GaAs, GaSb, InAs, and InSb monolayer structures are shown to be 1.85, 1.51, 1.44, and 1.32 eV respectively, which are larger than those of a zinc blende bulk phase structure with band gap values of 1.519, 0.822, 0.417, and 0.235 eV respectively.[1] The band gap of AlSb of our calculation is 1.97 eV, which is closed to the value in Ref. [38] with the same structure and GW0 method, but it is much smaller than 2.386 eV in Ref. [1], where the authors used a multi-band K·P method with a bulk structure. Other results of band gaps in our calculations are shown to be a little smaller than those in Ref. [38], where a more accurate method (GW0) was used but the variation trends are similar; thus we can use the data to conclude some regularity of electronic properties for the 25 kinds of binary compounds. It seems that the mechanical properties are quite radius dependent based on the analysis above. However, the band gaps have a similar trend when we intend to sort the band gaps according to the binary relative radii (not shown here). It is interesting that a new regularity exists in Table 1 for the band gaps; *i.e.*, if we ignore the B–V (V = N, P, As, Sb, Bi) except for BN and for a given V-column element, all band gaps will decrease monotonically with the increase of *III*-element row number in the periodic table (see Fig. 5 (a)). Conversely, for a given *III*-column element, a similar regularity is found except for Tl–V (V = N, P, As, Sb, Bi) and InN (see Fig. 5(b)). Figure 5(c) shows the relation between the band gap and relative radius (defined above). It is interesting that the band gaps monotonically decrease with the increase of relative radius, accompanied by periodic fluctuations, and the regularity in Fig. 5(c) is not the same as that in Fig. 3 although the y-axial values in both plots decrease monotonically in the overall trend. One can find in Fig. 5(c) that the valleys of all periodic fluctuations are always located at very special points, e.g. at BP (20), BAs (38), BSb (56), TlN (88), TlAs (114), and TlBi (164), among which the first three binary compounds are finally located at the positions with the same relative radius in the 25 compounds, while the last three are located at first at the positions with the same relative radius in the latter half of the 25 compounds (see Table 3). According to Fig. 5, it can be concluded that the band gaps for *III*–*V* binary compounds are group, period and radius dependent.

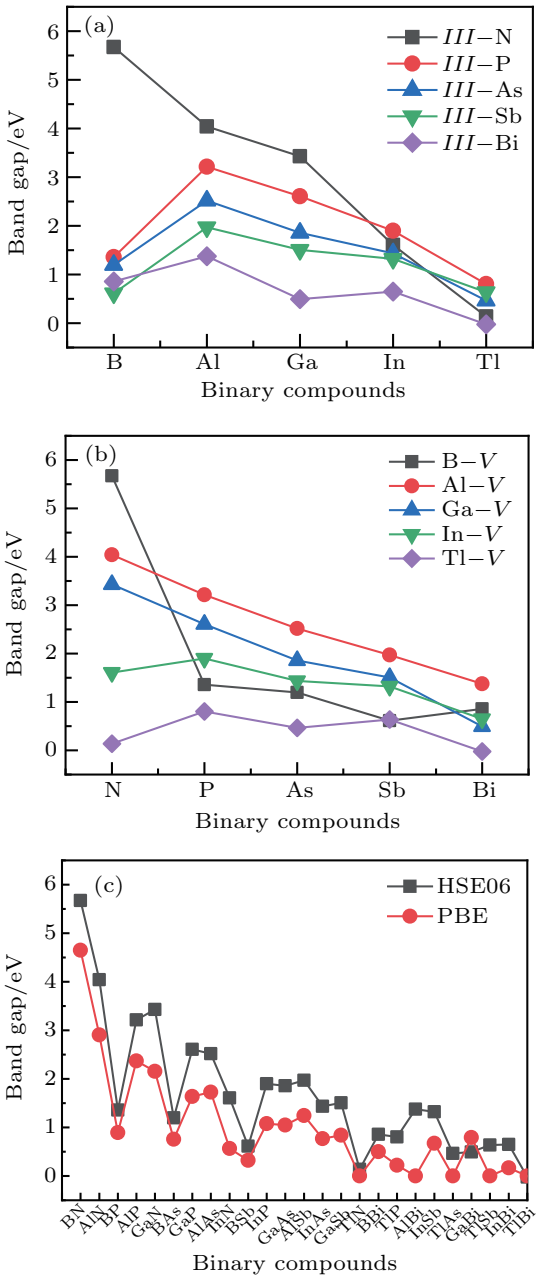


Fig. 5. Plots of band gap *versus* *III*–*V* binary monolayer compound, (a) for a given V-group element and varying the *III*-group element during different periods, (b) for varying a V-group element and a given *III*-group element, (c) and for the band gap versus all *III*–*V* binary compounds with a sorted relative radius.

The plots of effective mass of carrier versus different binary compounds are depicted in Figs. 6(a) and 6(b) for the effective mass of the electron and hole under a given *V* element and different *III* elements, respectively; the plots of effective mass of both carriers versus all *III*–*V* binary compounds under a radius sorted case are exhibited in Fig. 6(c); the plots of effective mass of carrier versus different binary compounds are shown in Figs. 6(d) and 6(e) for the effective mass of the electron and hole under a given *V* element and different *III* elements, respectively. We note that each effective mass in Fig. 6 is averaged by the two *K*-path directions at CBM or VBM in Table 1. As seen from Fig. 6(c), the effective mass values of the electron for most *III*–*V* binary compounds are very close to $0.25m_0$; a number of exceptions are found in a very small or very large radius region, while the effective mass of the hole is seen to be more sensitive before BSb and followed by a relative stable value close to $-0.5m_0$. One can find in Fig. 6(c) that a *III*–N binary will increase and a B–*V* binary will reduce the effective mass of the hole (AlN, BAs, *etc*.); *i.e*. almost all fluctuations of m_h are found to be at either a *III*–N or a B–*V* binary, which can be seen more clearly in Figs. 6(b) and 6(e). By investigating Figs. 6 (a) and 6(d), the effective mass of the electron of *III*–N and Tl–*V* are more sensitive with the increase of row numbers in the periodic table under a given N and Tl element respectively.

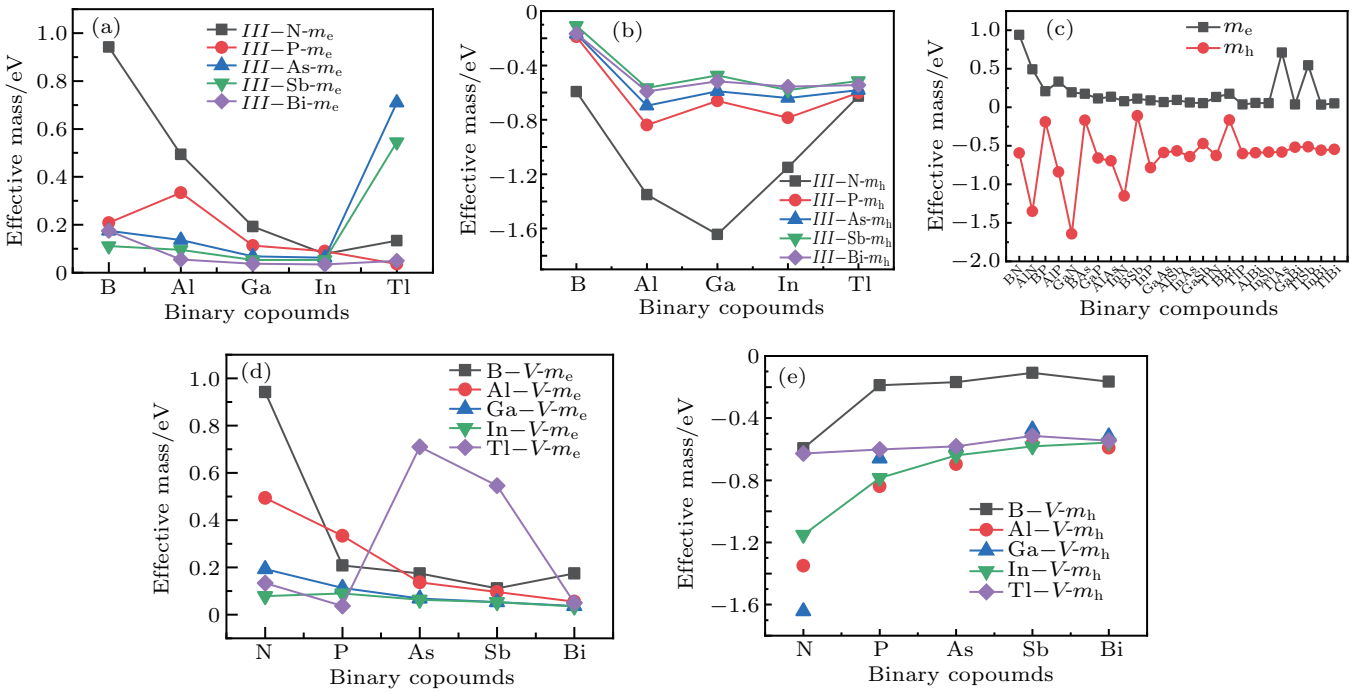


Fig. 6. Plots of effective mass of carrier *versus* binary compound, for effective mass of (a) electron and (b) hole under a given *V* element and different *III* elements, (c) for effective mass of both carriers *versus* all *III*–*V* binary compounds under a radius sorted case, and for effective mass of (d) electron and (e) hole under a given *V* element and different *III* elements, respectively.

We further calculate the band structures of 25 kinds of *III*–*V* binary monolayer compounds subjected to no strain with the HSE06 method as shown in Fig. 7. It follows from Fig. 7 that all bands are projected into s, p, and d orbitals for a clear investigation about the contributions of electrons. By analyzing the band structures of all the considered binary monolayer compounds, we find that there are 14 kinds of direct bands, 10 kinds of indirect bands and 1 kind of metal band. A most obvious regularity in Fig. 7 is that the binary monolayer compounds located in the top and left have a larger gap while the bottom and right ones have a smaller gap, which shows intuitive information for experimental researchers who intend to synthesize a new material with given band gaps based on *III*–*V* elements. It can be found in Fig. 7 that the shape of an *III*–N binary is much different from those of other *III*–*V* binaries in the same row; we infer from this point that an N element will dominate the band structure and hence the electronic properties for a give *III* element. Interestingly, a similar regularity is found in the case of B–*V* binaries; *i.e*., for a given *V* element in the same column, the shape of band structure of B–*V* is very different from those of other compounds. The VBM is found to be contributed by *V*-p electrons for all structures, while the CBM is more sophisticated. For instance, the CBM of BN is mainly contributed by N-s electrons while the CBM of GaN is mainly contributed by both Ga-s and N-s electrons. Another regularity found in Fig. 7 is that the conduction bands of the former 20 kinds of *III*–*V* binaries tend to shift downward to reduce the gaps while the remaining 5 kinds of *III*–*V* binary compounds located in the fifth row keep fixed relatively.

To investigate the effects of strain in different directions on the band properties of *III*–*V* monolayer structures, we calculate the uniaxial, equi-biaxial and shear strained band structures of all 25 kinds of *III*–*V* binary compounds at the PBE level rather than the HSE06 level. In this way we think it will be enough for us to investigate the change trend of the band structures in the case of strain. The most important reason for choosing a PBE level is that it consumes too much time for using a HSE06 level to calculate all 25 kinds of binaries

and 44 times for each one. For simplicity, we choose only 5 binaries, but all 10 elements are included as an example to show the regularity of the gaps under strain conditions in different directions; the results are shown in Fig. 8. It can be found in Fig. 8 that the band gaps are very dependent on the strain in different directions, and the anisotropic property in the band gap of AlP is in agreement with that of strain energy in Fig. 2(b); the band gaps of AlP and InSb *versus* equi-biaxial strain are seen to have a similar change trend while the band gap of GaAs decreases with a constant slope. The band gap of BN decreases either under a compressed or under a tensile equi-biaxial strain, and in the case of TlBi the band gap is not affected by the equi-biaxial strain. Analyzing the other 20 kinds of *III–V* binary compounds (not shown here), we find that there is generally not regularity on the whole, so we will not give more detailed discussion about Fig. 8., However, it is worth noting that by using the strains in different directions, one can tune the gaps of *III–V* binary monolayers very flexibly.

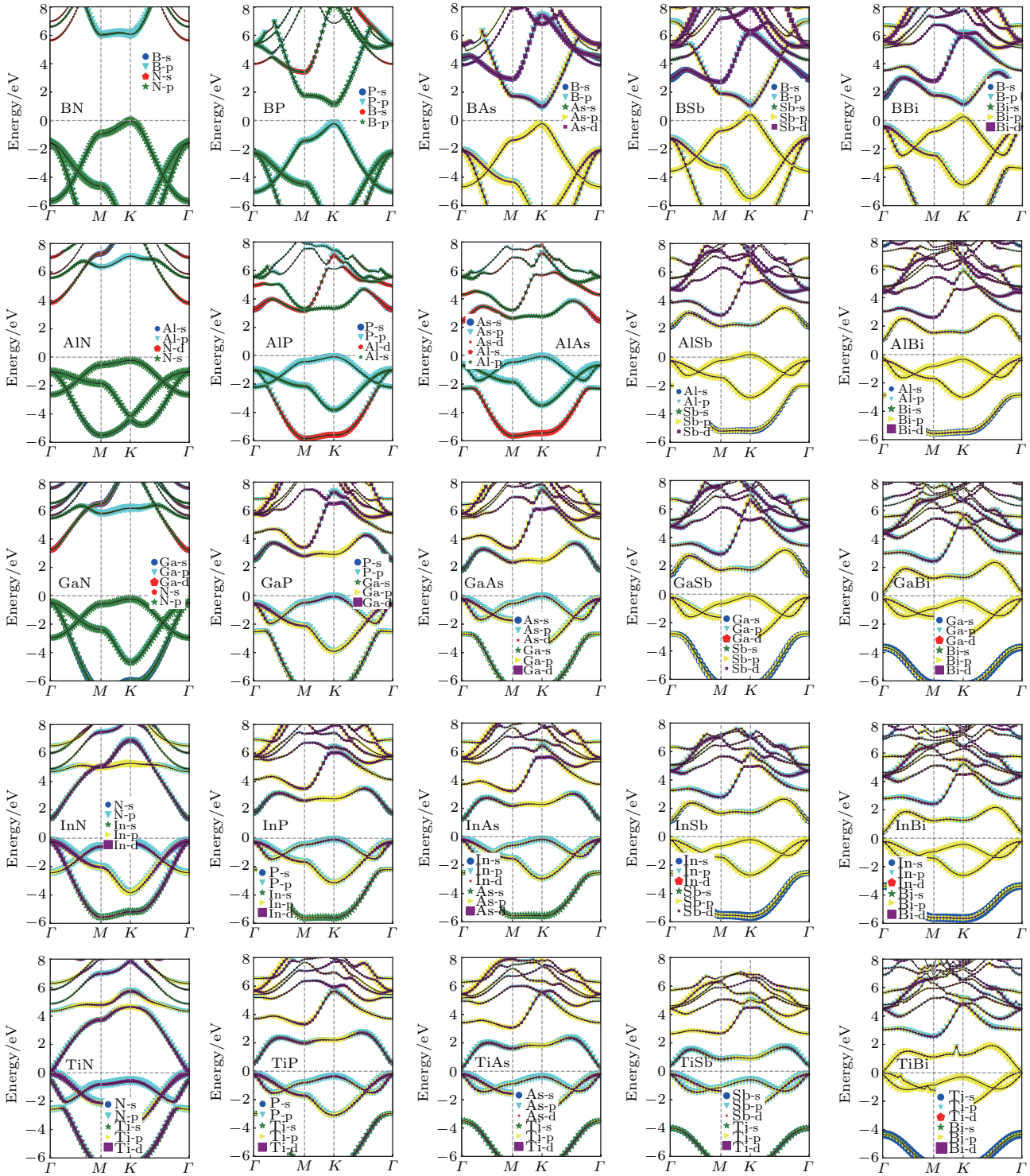


Fig. 7. Projected band structures of 25 kinds of *III–V* monolayer binary compounds calculated with the HSE06 method.

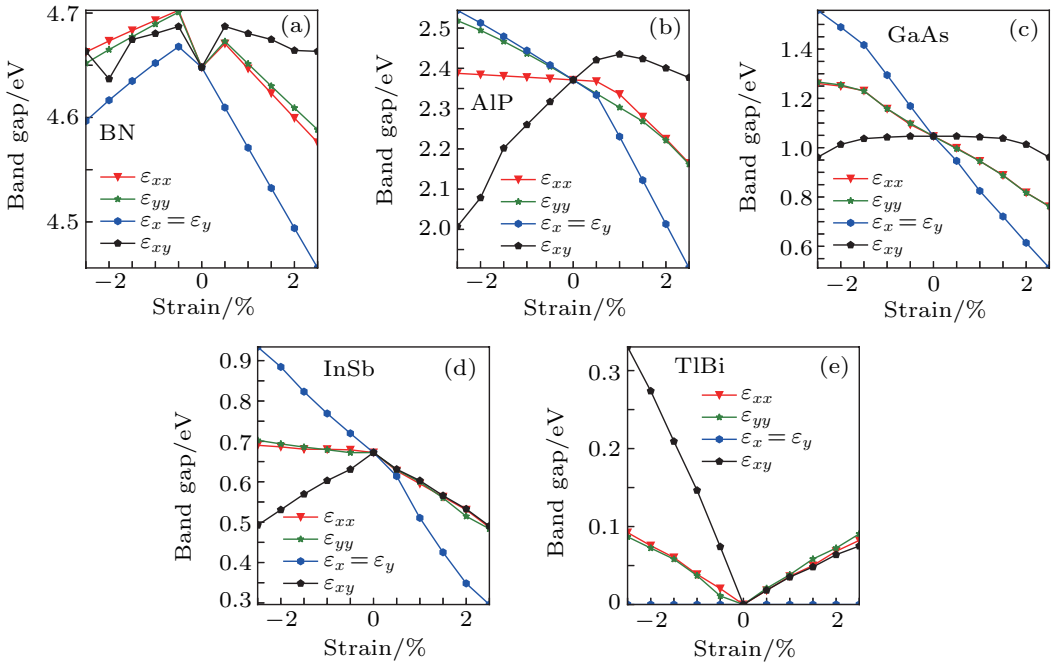


Fig. 8. Plots of band gap (PBE level) *versus* strain of five binaries *versus* the strain in different directions.

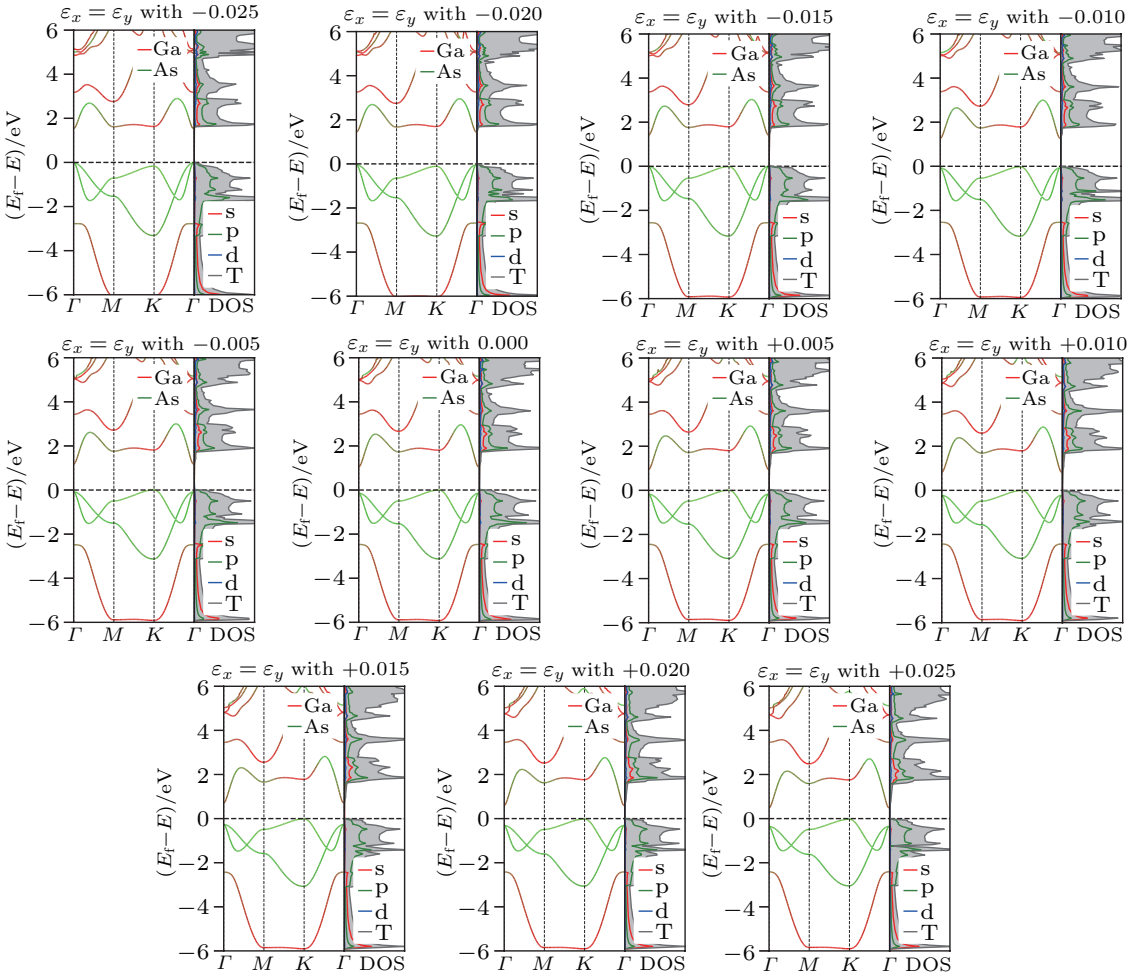


Fig. 9. The band structure and density of states of GaAs in different equi-biaxial strains from –0.025 to 0.025.

In order to show how the equi-biaxial strain can affect the band structure of a *III–V* binary compound, we take GaAs for example and the projected band structures and density of states of GaAs subjected to an equi-biaxial strain from −0.025 to 0.025, illustrated in Fig. 9. The results are in agreement with those in Ref. [20]. It can be found that the shape of band

structure of GaAs at the PBE level is the same as that at the HSE06 level in Fig. 7, which proves that our calculations at the PBE level are accurate enough in the case where we just want to discuss the trends of band structures under different strains. From Fig. 9, one can find that a compress strain will shift the VBM to a lower location and the CBM to a higher location, which means that the band gap increases and agrees with the results in Fig. 8. In the case of a tensile strain, it is a little different; *i.e.*, the VBM almost keeps fixed and the CBM is shifted to a lower location which leads the gap to decrease. From the partial density of states, we can know that the contribution of each orbital is nearly unaffected by the strain; *i.e.* under all different strains, the VBM is contributed by As(p) electrons and the CBM is contributed by Ga-s, As-s, and As-p electrons. It is worth noting that the equi-strain is able to not only shift the energy of CBM or VBM, but also change the type of band gap; *e.g.*, GaAs under no strain seems to be an indirect gap semiconductor and gradually changes into a direct band gap semiconductor under a -0.025 equi-strain. Similar results are found in the other 24 kinds of compounds but are not shown here for simplicity.

4. Conclusions

In this paper, by using first principle methods, we have performed calculations for 25 kinds of *III*–*V* binary monolayers, mainly including geometry parameters such as bond angle, bond length, and buckling constant, mechanical properties such as Young's modulus, stiffness constants, shear modulus, and Poisson's ratio, electronic properties such as band structures, density of states, and band edge carrier effective mass, and the formation energy of all binary compounds. By comparing the results of all 25 kinds of binary monolayers, some interesting and important regularities are found. By defining a relative radius according to the atomic number in the periodic table, we sort the 25 kinds of binary compounds from BN (12) to TlBi (164) based on the relative radius. We find the relative r radii of the 25 kinds of compounds exactly construct a symmetric matrix as seen in Table 3. As shown in Figs. 3 and 5, the mechanical properties and band gaps are dependent on the relative radius of the compound. It seems that mechanical properties and band gaps have a downward trend, on the whole, with an increase of relative radius. We find the Young's modulus for each of the 25 kinds of compounds varies linearly with the formation energy and is fitted to a linear relation. The effective mass of the hole of the *III*–N (*III* = Al, Ga, In, Tl) and B–*V* (*V* = P, As, Sb, Bi) binary is found to first decrease and then increase from an average value as seen from Fig. 6(c), while the effective mass of the electron is found to keep a relative stable value around $0.25m_0$, except with a few compounds. From the results of an HSE06 level calculation, the shape of the *III*–N and a B–*V* binaries are very different from that of other *III*- or -*V* binaries; we infer from this point that an N or a B element will dominate the band structure in this case and hence the electronic properties for a given *III*- or -*V* element binary. It is worth noting that B–*V* and *III*–N are exactly located in a symmetric location in Table 3; in our opinion, this is related to the particularity of effective mass of the hole and energy band structures of B–*V* and *III*–N binary compounds. Therefore, whether the physical properties of other *III*–*V* binary compounds at a symmetric position have similar correlations is worth studying further. By calculating the strained band structures of all 25 kinds of *III*–*V* binary compounds with the DFT level method, we find that both the CBM and VBM can be tuned by compress or tensile strains as well as the types of band gap.

References

[1] Vurgaftman I, Meyer J R and Ram-Mohan L R 2001 *J. Appl. Phys.* **89** 5815
[2] Bhattacharya P, Mi Z and Rahman A Z M S 2016 *Reference Module in Materials Science and Materials Engineering* (Elsevier)
[3] Hayrapetyan D B, Kazaryan E M and Sarkisyan H A 2016 *Opt. Commun.* **371** 138
[4] Weiner E C, Jakomin R, Micha D N, Xie H, Su P Y, Pinto L D, Pires M P, Ponce F A and Souza P L 2018 *Sol. Energy Mater. Sol. Cells* **178** 240
[5] Cardimona D A, Morath C P, Guidry D H and Cowan V M 2013 *Infr. Phys. Technol.* **59** 93
[6] Kim K, Lambrecht W R L and Segall B 1996 *Phys. Rev. B* **53** 16310
[7] Kern G, Kresse G and Hafner J 1999 *Phys. Rev. B* **59** 8551
[8] Ustundag M, Aslan M and Yalcin B G 2014 *Comput. Mater. Sci.* **81** 471
[9] Novoselov K S, Geim A K, Morozov S V, Jiang D, Zhang Y, Dubonos S V, Grigorieva I V and Firsov A A 2004 *Science* **306** 666
[10] Zhang Y, Tan Y W, Stormer H L and Kim P 2005 *Nature* **438** 201
[11] Jensen P J and Bennemann K H 2006 *Surf. Sci. Rep.* **61** 129
[12] Abergel D S L, Apalkov V, Berashevich J, Ziegler K and Chakraborty T 2010 *Adv. Phys.* **59** 261
[13] Ci L, Song L, Jin C H, Jariwala D, Wu D X, Li Y J, Srivastava A, Wang Z F, Storr K, Balicas L, Liu F and Ajayan P M 2010 *Nat. Mater.* **9** 430
[14] Song L, Ci L J, Lu H, Sorokin P B, Jin C H, Ni J, Kvashnin A G, Kvashnin D G, Lou J, Yakobson B I and Ajayan P M 2010 *Nano Lett.* **10** 3209
[15] Dong B J , Yang T, Wang J Z and Zhang Z D 2015 *Chin. Phys. B* **24** 096806
[16] Liu H, Neal A T, Zhu Z, Luo Z, Xu X F, Tomanek D and Ye P D 2014 *ACS Nano* **8** 4033
[17] Batmunkh M, Bat-Erdene M and Shapter J G 2016 *Adv. Mater.* **28** 8586
[18] Ren D H and Cheng X L 2012 *Chin. Phys. B* **21** 127103
[19] Beiranv R and Valedbagi S 2016 *Optik* **127** 1553
[20] Bahuguna B P, Saini L K, Sharma R O and Tiwari B 2018 *Phys. E* **99** 236
[21] Degheidy A R and Elkenany E B 2017 *Chin. Phys. B* **26** 086103
[22] Wang V, Ma N, Mizuseki H and Kawazoe Y 2012 *Solid State Commun.* **152** 816
[23] Wang V, Wu Z Q, Kawazoe Y and Geng W T 2018 *J. Phys. Chem. C* **122** 6930
[24] Wang V and Geng W T 2017 *J. Phys. Chem. C* **121** 10224
[25] Li J, Fan X, Wei Y, Wang V and Chen G 2016 *Chem. Phys. Lett.* **660** 244
[26] Kresse G and Furthmüller J 1996 *Phys. Rev. B* **54** 11169
[27] Kresse G and Furthmüller J 1996 *Comput. Mater. Sci.* **6** 15
[28] Blöchl P E 1994 *Phys. Rev. B* **50** 17953

[29] Perdew J P, Burke K and Ernzerhof M 1996 *Phys. Rev. Lett.* **77** 3865
[30] Monkhorst H J 1976 *Phys. Rev. B* **13** 5188
[31] Birch F 1947 *Phys. Rev.* **71** 809
[32] Noh J Y, Kim H and Kim Y S 2014 *Phys. Rev. B* **89** 205417
[33] Wang V, Xiao W, Ma D M , Liu R J and Yang C M 2014 *J. Appl. Phys.* **115** 043708
[34] Heyd J, Scuseria G E and Ernzerhof M 2003 *J. Chemical Physics* **118** 8207
[35] Grimme S 2006 *J. Computational Chemistry* **27** 1787
[36] Sanders N, Bayed D, Shi G S, Mengle K A and Kioupakis E 2017 *Nano Lett.* **17** 7345
[37] Xu Y N and Ching W Y 1991 *Phys. Rev. B* **44** 7787
[38] Şahin H, Cahangirov S, Topsakal M, Bekaroglu E, Akturk E, Senger R T and Ciraci S 2009 *Phys. Rev. B* **80** 155453
[39] Shunhong Z, Jian Z, Qian W, Xiaoshuang C, Yoshiyuki K and Puru J 2015 *Proc. Natl. Acad. Sci. USA* **112** 2372
[40] Zhong H, Huang K, Yu G and Yuan S 2018 *Phys. Rev. B* **98** 054104
[41] Peng Q, Ji W and De S 2012 *Comput. Mater. Sci.* **56** 11
[42] Shi L B, Zhang Y Y, Xiu X M and Dong H K 2018 *Carbon* **134** 103
[43] Li M M, Xiaofeng F and Zheng W T 2013 *J. Phys.: Condens. Matter* **25** 425502
[44] Becke A D 1993 *J. Chem. Phys.* **98** 1372
[45] Perdew J P, Ernzerhof M and Burke K 1996 *J. Chem. Phys.* **105** 9982
[46] Krukau A V, Vydrov O A, Izmaylov A F and Scuseria G E 2006 *J. Chem. Phys.* **125** 224106
[47] Marsman M, Paier J, Stroppa A and Kresse G 2008 *J. Phys.: Condens. Matter* **20** 064201